



# Integrative Analysis of Histopathological Images and Genomic Data in Colon Adenocarcinoma

Hui Li<sup>1,2†</sup>, Linyan Chen<sup>1,2†</sup>, Hao Zeng<sup>1†</sup>, Qimeng Liao<sup>1,2</sup>, Jianrui Ji<sup>1,2</sup> and Xuelei Ma<sup>1,2\*</sup>

<sup>1</sup> Department of Biotherapy, State Key Laboratory of Biotherapy, Cancer Center, West China Hospital, Sichuan University, Chengdu, China, <sup>2</sup> West China Hospital, West China School of Medicine, Sichuan University, Chengdu, China

## OPEN ACCESS

### Edited by:

Francesca De Felice,  
Sapienza University of Rome, Italy

### Reviewed by:

Katia Pane,  
Institute of Research and Medical Care  
(IRCCS) SDN, Italy  
Izilda Cardinalli,  
Centro Infantil Boldrini, Brazil

### \*Correspondence:

Xuelei Ma  
drmaxuelei@gmail.com

<sup>†</sup>These authors have contributed  
equally to this work and  
share first authorship

### Specialty section:

This article was submitted to  
Gastrointestinal Cancers,  
a section of the journal  
Frontiers in Oncology

**Received:** 01 December 2020

**Accepted:** 31 August 2021

**Published:** 27 September 2021

### Citation:

Li H, Chen L, Zeng H, Liao Q,  
Ji J and Ma X (2021) Integrative  
Analysis of Histopathological  
Images and Genomic Data in  
Colon Adenocarcinoma.  
*Front. Oncol.* 11:636451.  
doi: 10.3389/fonc.2021.636451

**Background:** Colon adenocarcinoma (COAD) is one of the most common malignant tumors in the world. The histopathological features are crucial for the diagnosis, prognosis, and therapy of COAD.

**Methods:** We downloaded 719 whole-slide histopathological images from TCIA, and 459 corresponding HTSeq-counts mRNA expression and clinical data were obtained from TCGA. Histopathological image features were extracted by CellProfiler. Prognostic image features were selected by the least absolute shrinkage and selection operator (LASSO) and support vector machine (SVM) algorithms. The co-expression gene module correlated with prognostic image features was identified by weighted gene co-expression network analysis (WGCNA). Random forest was employed to construct an integrative prognostic model and calculate the histopathological-genomic prognosis factor (HGPF).

**Results:** There were five prognostic image features and one co-expression gene module involved in the model construction. The time-dependent receiver operating curve showed that the prognostic model had a significant prognostic value. Patients were divided into high-risk group and low-risk group based on the HGPF. Kaplan-Meier analysis indicated that the overall survival of the low-risk group was significantly better than the high-risk group.

**Conclusions:** These results suggested that the histopathological image features had a certain ability to predict the survival of COAD patients. The integrative prognostic model based on the histopathological images and genomic features could further improve the prognosis prediction in COAD, which may assist the clinical decision in the future.

**Keywords:** colon adenocarcinoma, histopathological features, genomic data, random forest, prognosis

## INTRODUCTION

Colon adenocarcinoma (COAD) is the second most frequent malignancy in developed countries (1). In recent years, the incidence of COAD has been rising around the world. Although the survival rate of COAD has been improved greatly in the recent years, even in the European countries with the highest survival rate, the 5-year survival rate is no more than 60% (2). Currently, the most effective and recognized therapy of COAD is radical resection. Adjuvant treatment is designed to assist radical surgery, reduce the risk of recurrence, and improve the survival rates (3). Among the potential factors affecting the prognosis of COAD, the depth of tumor infiltration into the intestinal wall and the involvement of lymph nodes are the most important, which are also the basis of the clinical staging system (4). Therefore, accurate pathological diagnosis based on histopathological sections is critical for the prognostic prediction and therapy strategies of COAD.

Histopathological images contain a great deal of information about tumors, including the nature of the lesions, histological classification, and grade of malignancy. Therefore, histopathological diagnosis is often regarded as the gold standard, and has an irreplaceable status in clinical practice (5). Nevertheless, in many regions of the world, the number of pathologists and the services they are able to provide may not meet the needs of an adequate pathological diagnosis (6). The research and development of the digital whole slide imaging (WSI) system enable pathological sections to be read digitally, breaking the limitations of traditional microscopes. In addition, the application of computer aided diagnosis (CAD) based on the histopathological images promotes the intellectuality of pathological diagnosis, and thereby improves the diagnostic efficiency and accuracy (7). The computerized intelligent histopathologic image analysis system has been applied to breast (8), lung (9, 10), colon (11), and prostate (12) cancers due to its potential to identify novel tumor biomarkers.

The advantages of histopathological images in the prediction of tumor prognosis have been widely recognized. However, considering the complexity of molecular mechanisms affecting tumor prognosis, single-source predictors are far from adequate in prognostic modeling. Researchers have attempted to combine predictors from multiple sources to improve tumor prognostic models. For the past few years, the widespread application of high-throughput sequencing technology has promoted the research of serial analysis of gene expression, so that gene expression characteristics can be used for the prognosis prediction in cancers (13, 14). The information revealed by the cancer omics profile and histopathological images is not only relatively independent but also has commonality to a certain extent. The morphological features of tumor cells and histological structure of the tumor microenvironment can be influenced by molecular changes, individual immune function, and environment (15–17). For instance, a previous study (18) has found that there is a significant correlation between the TP53 mutation and pathological characteristics of tumor cells in lung adenocarcinoma. Another study demonstrated the correlation between the amplifications of PDGFRA, EGFR, MDM2, and specific image features in glioblastoma (19). Some researchers

have combined radiomics and genomics to predict the clinical outcomes of cancers (20–22). For example, Schiano C. et al. integrated imaging parameters from hybrid 18F-FDG-PET/MRI with the expression level of Yin Yang 1 to predict early metastases of breast cancer (20). It is also feasible to combine the histopathological features with cancer omics to optimize the prognostic models. At present, the prognostic models based on the genomic data and histopathological image features have obtained a superior prediction performance in renal cell carcinoma (23), breast cancer (24), and other early-stage cancers (25), etc.

In this study, all of the whole-slide histopathological images were downloaded from The Cancer Imaging Archive (TCIA, <http://www.cancerimagingarchive.net/>) database and cropped into 1,000 x 1,000 pixel sub-images. TCIA collects, provides, and manages affluent cancer image data supported by 28 agencies, and can provide researchers with publicly available imaging data and unique imaging resources (26, 27). The mRNA expression profiles and clinical data of COAD patients were attained from The Cancer Genome Atlas (TCGA, <https://portal.gdc.cancer.gov/>) database. TCGA is one of the largest and richest publicly funded projects designed to build a comprehensive genetic map of the cancer genome (28). We extracted the histopathological image features through CellProfiler, an open-source modular image analysis software. CellProfiler can convert color image into grayscale and extract a number of features from identified cells or subcellular regions, including size, shape, intensity, and texture. We used the least absolute shrinkage and selection operator (LASSO) and support vector machine (SVM) models to identify the pathological features correlated with prognosis. Totally, five prognostic features were obtained by taking the intersection of the pathological features filtrated by the two algorithms. To further explore the potential correlation between the pathological and genomic features of COAD, we performed weighted gene co-expression network analysis (WGCNA) to identify the co-expression gene module that correlated most with the prognostic pathological image features. Finally, we utilized the random forest (RF) method to integrate the pathological features and genomic data to establish an integrative prognostic model and validated the model by the test set.

## MATERIALS AND METHODS

### Data Source and Downloads

Totally, 719 whole slide histopathological images of 218 patients were downloaded from TCIA. The histopathological tissue slides were all formalin-fixed and paraffin-embedded to preserve the cell morphology as much as possible, ensuring that they were suitable for image feature recognition.

The mRNA expression data of HTSeq-count and clinical information of COAD patients were downloaded from TCGA. In total, we obtained 478 samples with mRNA sequencing data from TCGA, and 459 of them had clinical information. There were 19,754 genomic features in each sample (**Table S1**). Variance-stabilizing transformation (VST) was used to

normalize the mRNA sequencing data with the R package DESeq2 for further analysis in WGCNA.

## Extraction of Histopathological Imaging Features

The flowchart of processing histopathological images, extracting imaging features, and establishing an integrative prognostic model is shown in **Figure 1**.

In order to extract the image features from the whole slide histopathological images, the image processing procedure consisted of three steps. Firstly, since the size of each pathological image was too large to be used directly for feature extraction, we cropped each image evenly into  $1,000 \times 1,000$  pixels sub-images and saved them in tiff image format using Openslide Python library (29). In this process, sub-images containing more than 50% white background were excluded. To eliminate the sample selection bias and reduce computing amount, we randomly selected 20 sub-images from the remaining sub-images for the next step. Cropping and random selection of images have been widely used in the processing of the whole slide images (9, 18, 24).

Secondly, we applied CellProfiler (30) to extract features from each sub-image. The hematoxylin-eosin staining makes the cell nuclei and cytoplasm appear different colors in the histopathological images. A total of 656 features were the output for each sub-image. These features were different from the well-known classical pathological characteristics such as cellular basophilic, eosinophilic, nuclear atypia, and mitotic counts, which cannot be recognized by visual inspection. After further removing irrelevant features such as file sizes and execution information, 590 features were used in the following workflow.

Thirdly, we calculated the average value of 590 features extracted from 20 sub-images for each slide. When a patient had more than one slide, the mean values over those slides were further calculated.

It should be emphasized that the purpose of our study was not to concretely explain the relationship between these image features and COAD, but to quest the optimal combination of features to establish an integrative prognostic model of COAD. Therefore, the lack of definite biological interpretations would not prevent us from conducting further reasonable analysis.

## Acquisition of Prognosis-Related Features

By using the R package “e1071” and “glmnet” on the R version 3.6.3 software, the support vector machines recursive feature elimination (SVM-RFE) and LASSO-Cox algorithms were employed to filtrate the prognostic image features most correlated with the prognosis of COAD. Here, we used 5-fold cross-validation in both the LASSO-Cox and SVM-RFE algorithms. LASSO constructs a penalty function, and compresses the insignificant variable coefficient to 0 to achieve the purpose of variable selection. By customizing the optimal value of the parameter lambda ( $\lambda$ ), the user can control the balance between the sparsity (how many features are produced) and high prediction accuracy and minimum cross validation error. Image features with nonzero coefficients were finally regarded as the prognostic features and used to fit the regression model.

SVM-RFE is a backward feature selection machine learning method on the basis of SVM. In the training set, SVM-RFE ranked the pathological image features in a descending order of importance, iteratively eliminated the minimum features, and trained the model with the remaining features until all features were removed. When running the 5-fold cross-validation on SVM-RFE, feature selection was performed by defining the high-risk (survival time less than 12 months) and low-risk patients (survival time more than 60 months) as the training samples. In the SVM-RFE model, the maximal cross-validated accuracy was adopted as the evaluation index to confirm the optimal feature subset related to the prognosis. The optimal subset of features obtained by SVM-RFE was intersected with the results of LASSO regression to obtain the pathological features most relevant to the prognosis.

## Co-Expression Gene Module Analysis

WGCNA is an effective means to identify the co-expression gene modules by clustering the highly correlated genes, and perform correlation analysis between the modules and phenotypes to explore the potential marker genes of cancer (31). Based on the normalized mRNA profiles, WGCNA was employed to construct the co-expression gene network and explore the co-expressed gene module most correlated with the pathological prognostic features defined by machine learning algorithms. We calculated the interaction coefficient between genes and then computed the topological overlap measure (TOM) using the adjacency matrix. The co-expression network was constructed based on the *W* matrix to determine the co-expression gene modules. During this process, modules with statistical significance ( $p < 0.05$ ) were regarded as prognosis-related modules. To further explore the interrelationship among the genes in the prognosis-related modules, we performed Gene Ontology (GO) enrichment analysis with Metascape (<http://metascape.org>). In this process, default thresholds were applied for pathway analysis.

## Establishment of an Integrative Prognostic Model

Based on the histopathological features and genomic data of COAD patients, we applied random forest algorithms with 1,000 decision trees by the R “randomForestSRC” package to construct an integrative prognostic model. RF is a classifier containing multiple decision trees and each tree is built on an independent bootstrap training set. The output category is determined by the mode of the output category of individual trees. RF has great advantages over other algorithms in high-dimensional data processing. It can process high-dimensional data without deleting variables, and can evaluate the predictive ability of each feature. Meanwhile, the unbiased estimation of the generalization error generated by internal cross validation ensures high accuracy. The randomness of training samples for each decision tree and the selection of variables for splitting at each node can reduce overfitting.

The samples were randomly divided into 10 parts, including 7 parts of the training set ( $n = 140$ ) and 3 parts of the test set ( $n = 59$ ). The ratio of 7:3 is commonly used in machine learning algorithms (32–34). The 10-fold cross-validation was used during model constructing. Based on the training set, we constructed the

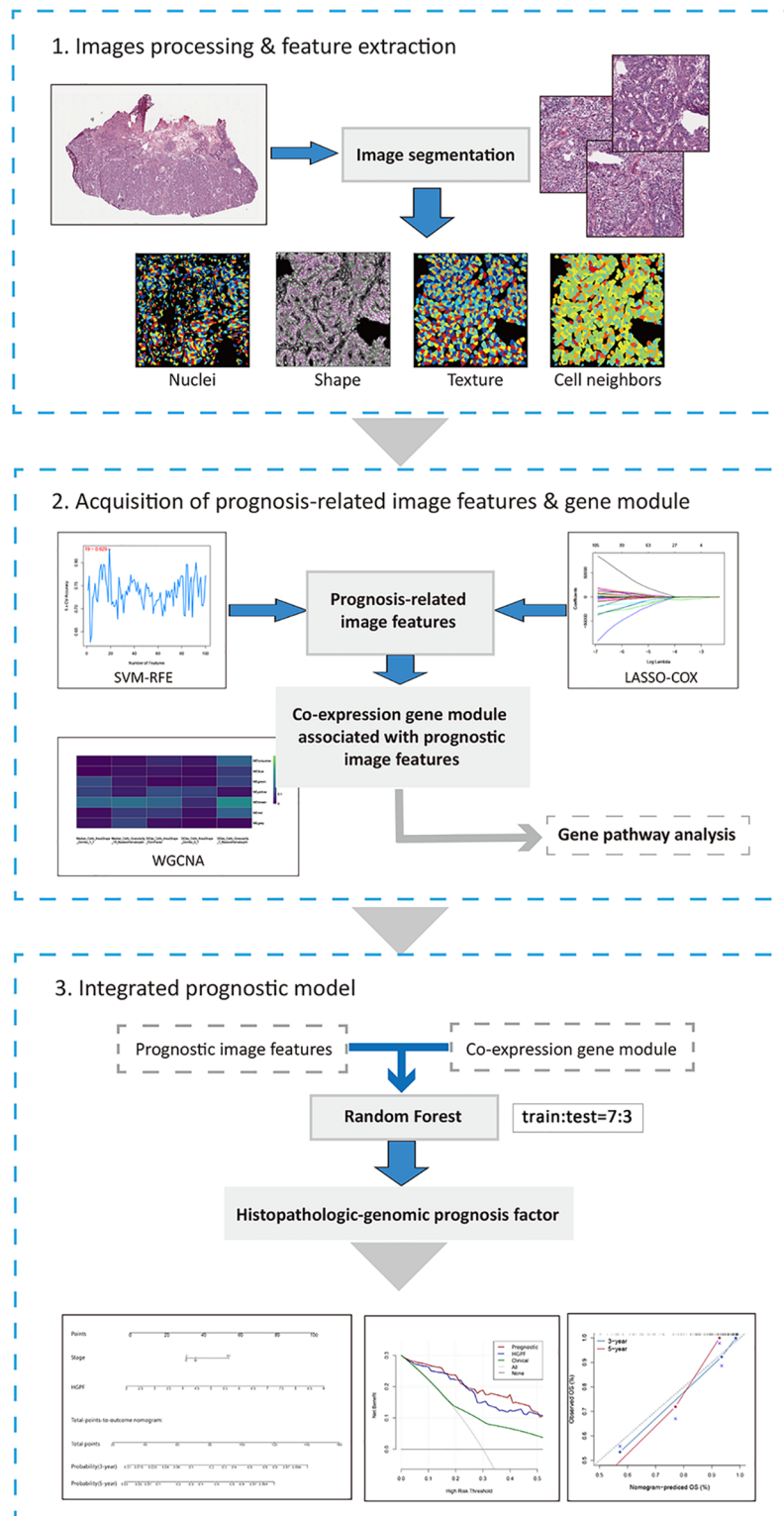


**FIGURE 1** | The workflow chart of key steps in this study. The whole-slide histopathological images of colon cancer were evenly cropped into sub-images of 1000×1000 pixels. After processing and selecting these sub-images, several image features were extracted by CellProfiler for further analysis. Then, LASSO-COX regression and SVM-RFE were performed to acquire prognosis-related image features. And WGCNA was used to identify co-expression gene modules associated with prognostic features. Histopathological features and genomic data were integrated into histopathological-genomic prognosis factor (HGPF) by random forest method with 10-fold cross-validation (the sample ratio of training set and test set is 7:3). Performance of the prediction model was evaluated.

integrative prognostic model with the pathological image features and mRNA expression profiles, which was defined as the histopathological-genomic prognosis factor (HGPF) model. The test set was then used to validate the prediction performance of the HGPF model. Afterwards, time-dependent receiver operating characteristic (ROC) curve was plotted and the 1-, 3-, and 5-year area under curves (AUCs) were calculated according to the average accuracies of the 10-fold cross-validation. We then used the RF model to estimate the survival risk of each patient and obtain the risk score of each patient. Based on the median of the risk score, the training set and test set can be divided into the high-risk score group and low-risk score group, respectively. Kaplan-Meier analysis and the log-rank test was used to compare the survival difference between the two groups.

After univariate Cox regression, we incorporated meaningful results ( $p < 0.05$ ) into the multivariate Cox regression analysis. Two predictive factors, HGPF and tumor stage of patients, were used in the development of the prognostic nomogram. In the nomogram, scores were assigned to the predictive factors according to the impact of the predictors on the survival outcome (the value of regression coefficient). Finally, the total score of each patient was associated with the survival probability through the function conversion.

## RESULT

### Patient Characteristics

A total of 199 COAD patients (112 male and 87 female) were included in this study. Histopathological images, mRNA expression data, and clinical information were downloaded from TCIA and TCGA. The median age of patients at first diagnosis was 71.0 years old (range 36–89 years). There were 167 patients who

survived and 32 patients who died at the last follow-up. The median survival time was 24.5 months. Patient characteristics are shown in **Table 1** and detailed clinical information of patients are shown in **Table S2**.

### Acquisition of Histopathological Images Features

CellProfiler transforms color images into grayscale images and measures image features from 10 aspects, including the correlation between intensities in different images, image area occupied, image granularity, image intensity, image quality, object intensity, object neighbors, object radial distribution, object size, shape, and texture. Texture reflects the degree and nature of the image or object textures through measuring the intensity variations in grayscale images. Image granularity is a texture measurement that outputs the spectra of the fitting degree between the size measures of the structure elements and image texture. Object size shape measures several area and shape features of each identified object in the image, such as area, perimeter, formfactor, solidity, Euler's number, and orientation. For example, form factor measures the object shape with the formula " $4 * \pi * \text{Area} / \text{Perimeter}^2$ ". Zernike shape features contain a series of 30 shape features based on Zernike polynomials from order 0 to order 9.

Finally, we extracted 590 image features from each sub-image and calculated the average value of representative sub-images for each corresponding slide.

### Prognosis-Related Features Identification and Co-Expression Gene Module Selection

The results of data dimension reduction through LASSO-Cox and SVM-RFE are shown in **Figure 2**. The optimal subset of

**TABLE 1** | Demographic and clinical characteristics of patients.

Characteristic	Total (n = 199)	Train (n = 140)	Test (n = 59)	P-value
Age: median (range)	71.0 (36–89)	72.0 (36–89)	68.0 (41–86)	0.599
Gender				
Male	112 (56.3%)	78 (55.7%)	34 (57.6%)	0.876
Female	87 (43.7%)	62 (44.3%)	25 (42.4%)	
T classification				
T1–T2	39 (19.6%)	25 (17.9%)	14 (23.7%)	0.336
T3–T4	160 (80.4%)	115 (82.1%)	45 (76.3%)	
N classification				
N0	124 (62.3%)	84 (60.0%)	40 (67.8%)	0.339
N1–N2	75 (37.7%)	56 (40.0%)	19 (32.2%)	
M classification				
M0	151 (75.9%)	105 (75.0%)	46 (78.0%)	0.690
M1	29 (14.6%)	20 (14.3%)	9 (15.3%)	
Mx	15 (7.5%)	12 (8.6%)	3 (5.1%)	
NA	4 (2%)	3 (2.1%)	1 (1.7%)	
TNM stage				
I–II	115 (57.8%)	78 (55.7%)	37 (62.7%)	0.523
III–IV	78 (39.2%)	57 (40.7%)	21 (35.6%)	
NA	6 (3.0%)	5 (3.6%)	1 (1.7%)	
OS(d): median	735.0	737.5	731.0	0.448
Event				
Alive	167 (83.9%)	114 (81.4%)	53 (89.8%)	0.204
Dead	32 (16.1%)	26 (18.6%)	6 (10.2%)	

features determined by the maximal cross-validated accuracy contained 19 features after feature elimination by the SVM-RFE algorithm. The LASSO-Cox regression identified eight prognostic features. We then intersected the results of the two algorithms to obtain five features (two Zernike shape features, two Granularity features, and one formfactor feature), which were defined as the prognostic image features of COAD. The examples of selected histopathological sub-images in both high-risk and low-risk groups are presented in **Figure 3**. To identify the co-expression gene modules with prognostic significance, WGCNA was applied to evaluate the relationship between the five prognostic image features and co-expression gene modules. The strength of association was represented by different colors (**Figure 4**). Obviously, the brown module containing 372 genes had the most outstanding association with the image features. Therefore, the brown module was selected as the key module with prognostic significance to build the integrative prognostic model.

### Enrichment Analysis of the Key Gene Module

**Figure 5A** lists the top 20 GO terms that were significantly enriched. The interrelationship among the 372 genes and their respective pathways is shown in **Figure 5B**. The results indicated that there were significant intrinsic associations among the biological function of these genes. In addition, most of them were enriched in biological processes such as blood vessel development, heart development, skeletal system development, and tissue morphogenesis. Several cellular components were also related, such as extracellular matrix (ECM) organization, ECM proteoglycans, and supramolecular fiber organization. Detailed enrichment results of 372 genes are shown in **Table S3**.

### Construction and Validation of the Integrative Prognostic Model

The COAD patients were randomly divided into the training set (n = 140) and test set (n = 59). We next established a prognostic

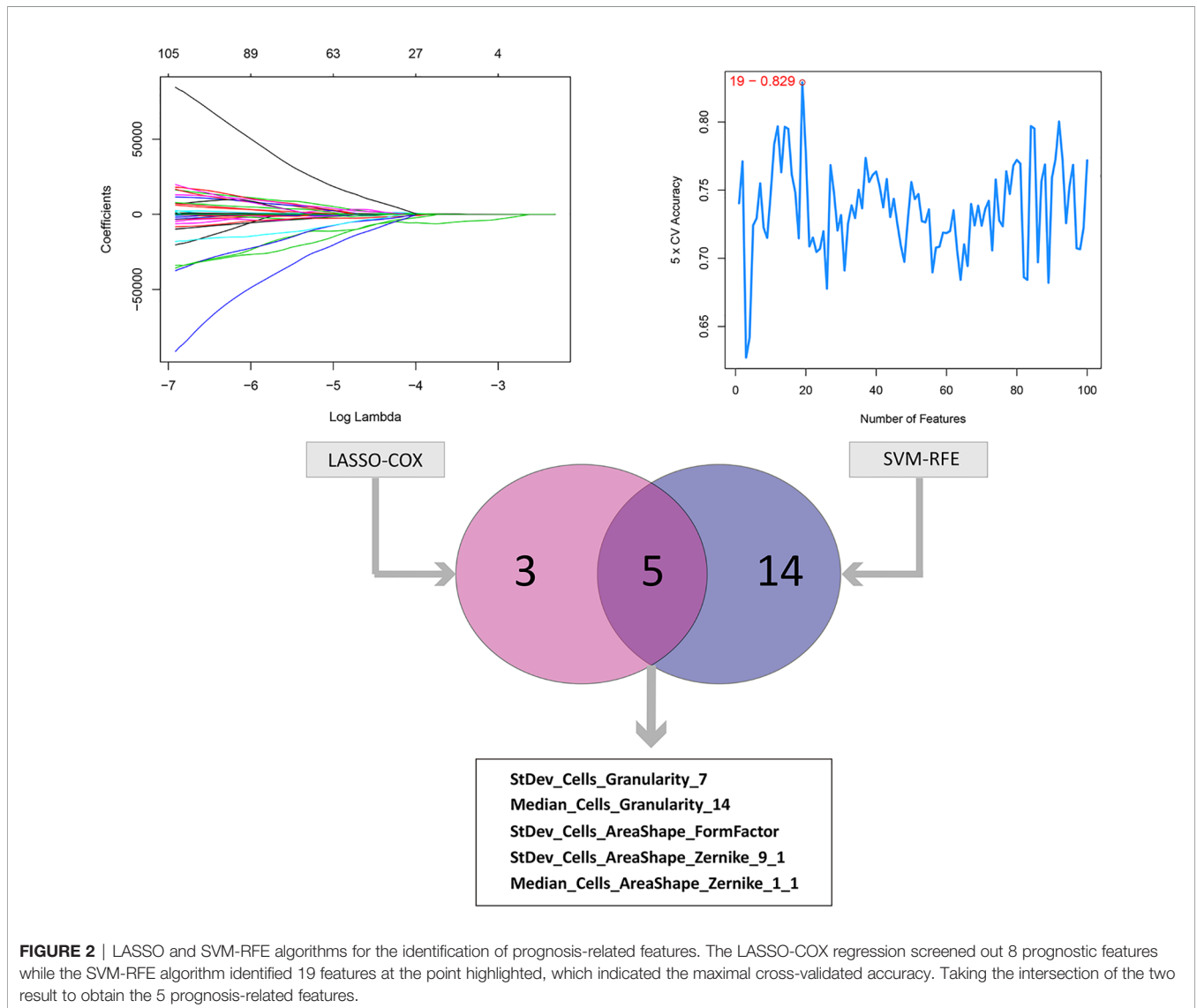


**FIGURE 2** | LASSO and SVM-RFE algorithms for the identification of prognosis-related features. The LASSO-COX regression screened out 8 prognostic features while the SVM-RFE algorithm identified 19 features at the point highlighted, which indicated the maximal cross-validated accuracy. Taking the intersection of the two result to obtain the 5 prognosis-related features.

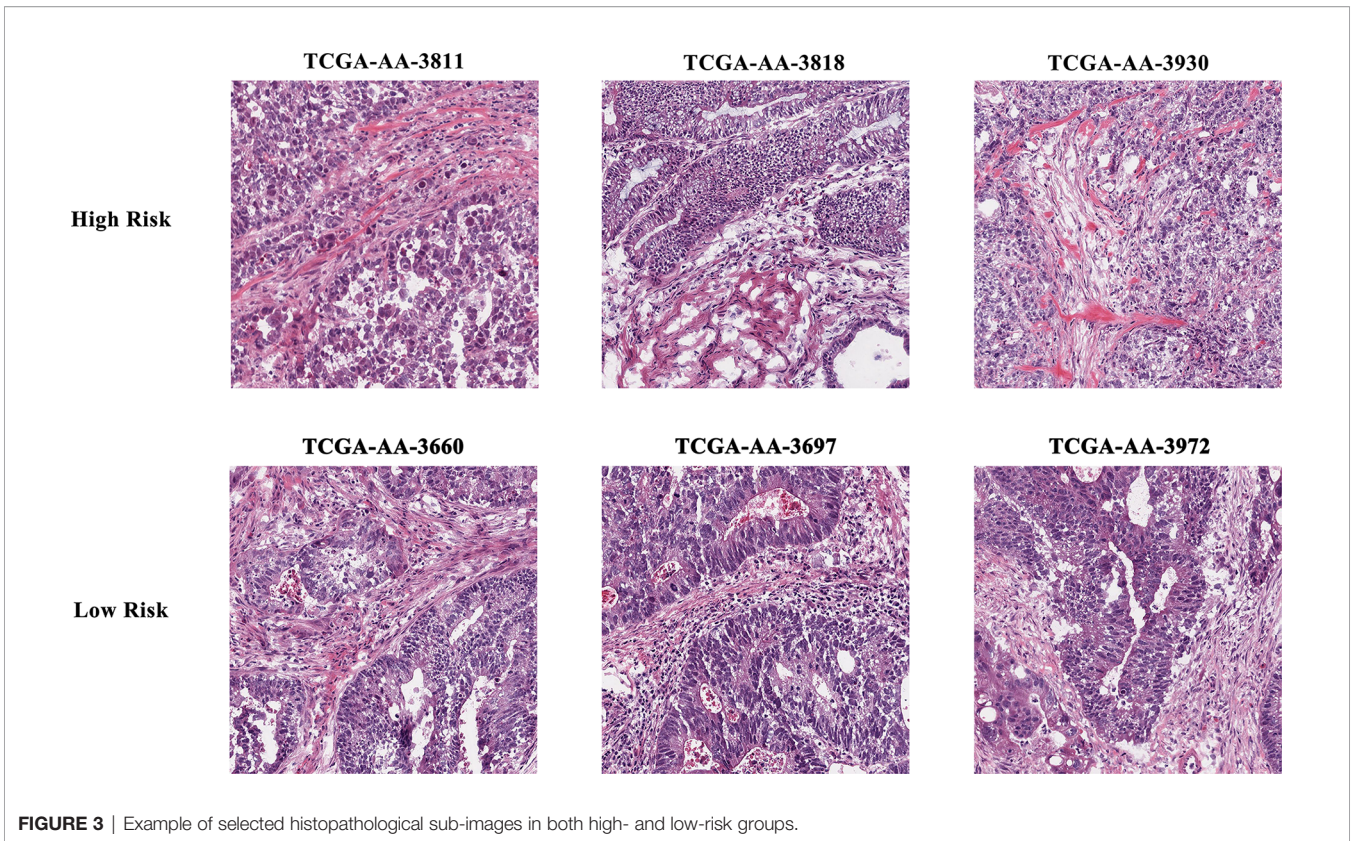


**FIGURE 3** | Example of selected histopathological sub-images in both high- and low-risk groups.

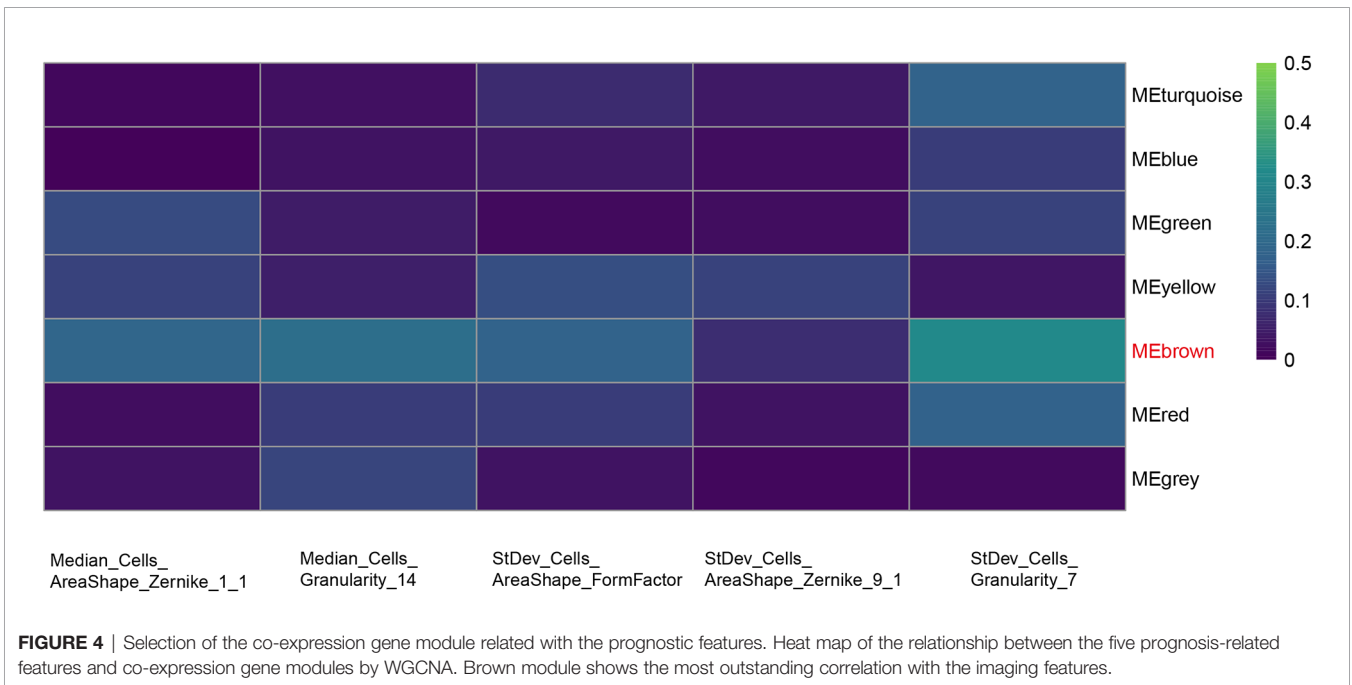


**FIGURE 4** | Selection of the co-expression gene module related with the prognostic features. Heat map of the relationship between the five prognosis-related features and co-expression gene modules by WGCNA. Brown module shows the most outstanding correlation with the imaging features.

model using the prognostic image features and gene module in the training set, and validated its predictive value in the test set. The development of a random forest model and the importance of six variables are shown in **Figure 6**. Since the survival results include both the survival state and survival time, the time-

dependent ROC curve can more comprehensively describe the predictive ability of the model over time. In the training set, the 1-, 3-, and 5-year AUCs were 0.948, 0.916, and 0.933 respectively (**Figure 7A**). In the test set, the 1-, 3-, and 5-year AUCs were 0.913, 0.894, and 0.924, respectively (**Figure 7B**). The predictive

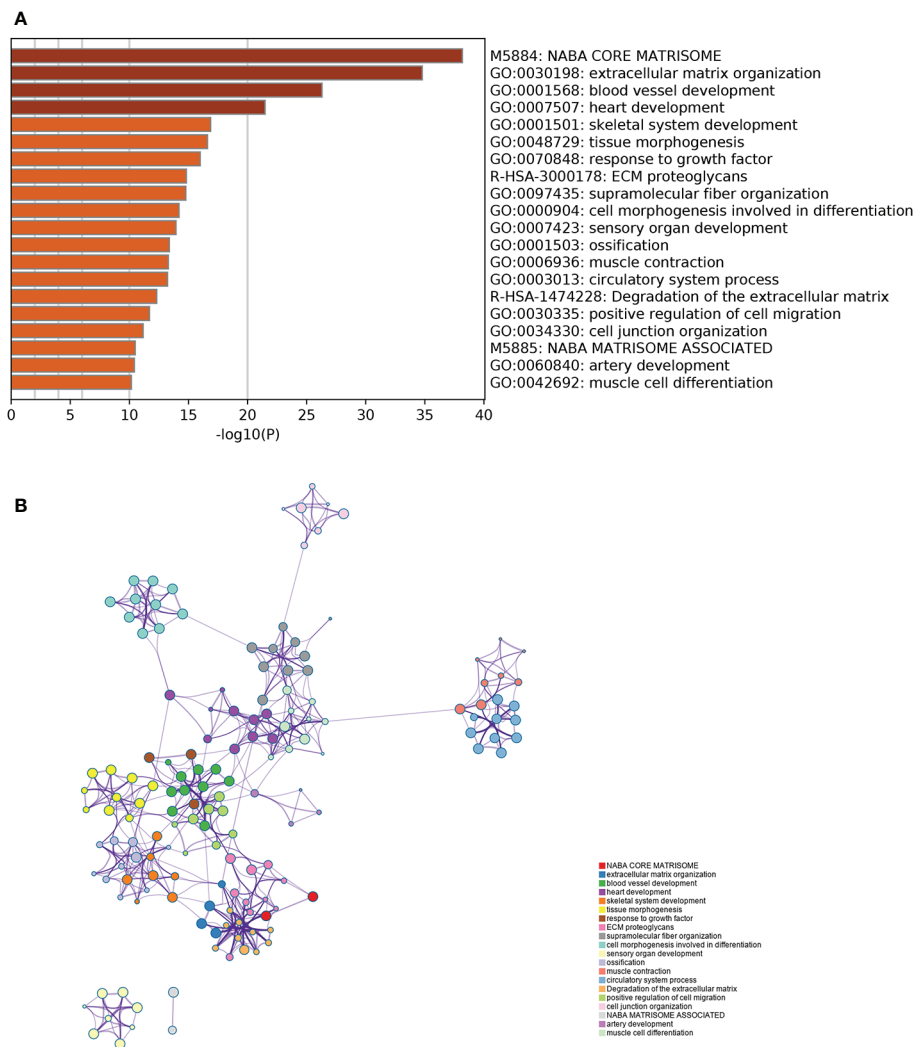


**FIGURE 5** | Gene Ontology enrichment analysis of the key gene module. **(A)** The top 20 GO terms which were significantly enriched. **(B)** The interrelationship and intrarerelationship among the cluster of enriched terms. Each dot represents one term, and the color annotates its cluster identity.

accuracy of the test set remained at a high level. Whereafter, patients were divided into the high-risk group and low-risk group by the median value of HGPF. The detailed results of random forest for the training set and test set are shown in the **Supplementary Material (Tables S4, S5)**. The results of the Kaplan-Meier analysis demonstrated that the overall survival rate of low-risk score patients was significantly better than that of high-risk score patients in both the training set ( $p < 0.0001$ , **Figure 7C**) and test set ( $p = 0.00018$ , **Figure 7D**).

A nomogram scoring system incorporating the HGPF and tumor stage of patients was constructed using the Cox regression model (**Figure 8A**). Patients were scored according to the weights of the two predictors, and the 3- and 5-year overall survival probabilities were predicted. The calibration curve demonstrated that the nomogram had a high fitting degree for the prediction of the 3- and 5-year overall survival compared to

the actual outcomes (**Figure 8B**). Moreover, decision curve analysis (DCA) was used to evaluate the clinical benefit of each model, including the integrative prognostic model (HGPF risk score combined with tumor stage), HGPF model, and clinical model. The integrated model had a better net benefit than others in the DCA analysis (**Figure 8C**).

## DISCUSSION

In this study, we extracted image features from whole-slide histopathological images by CellProfiler and identified five prognostic image features with machine learning algorithms. We also identified a prognosis-related module by establishing a gene co-expression network. We detected significant intrinsic associations among the biological function of the genes in a

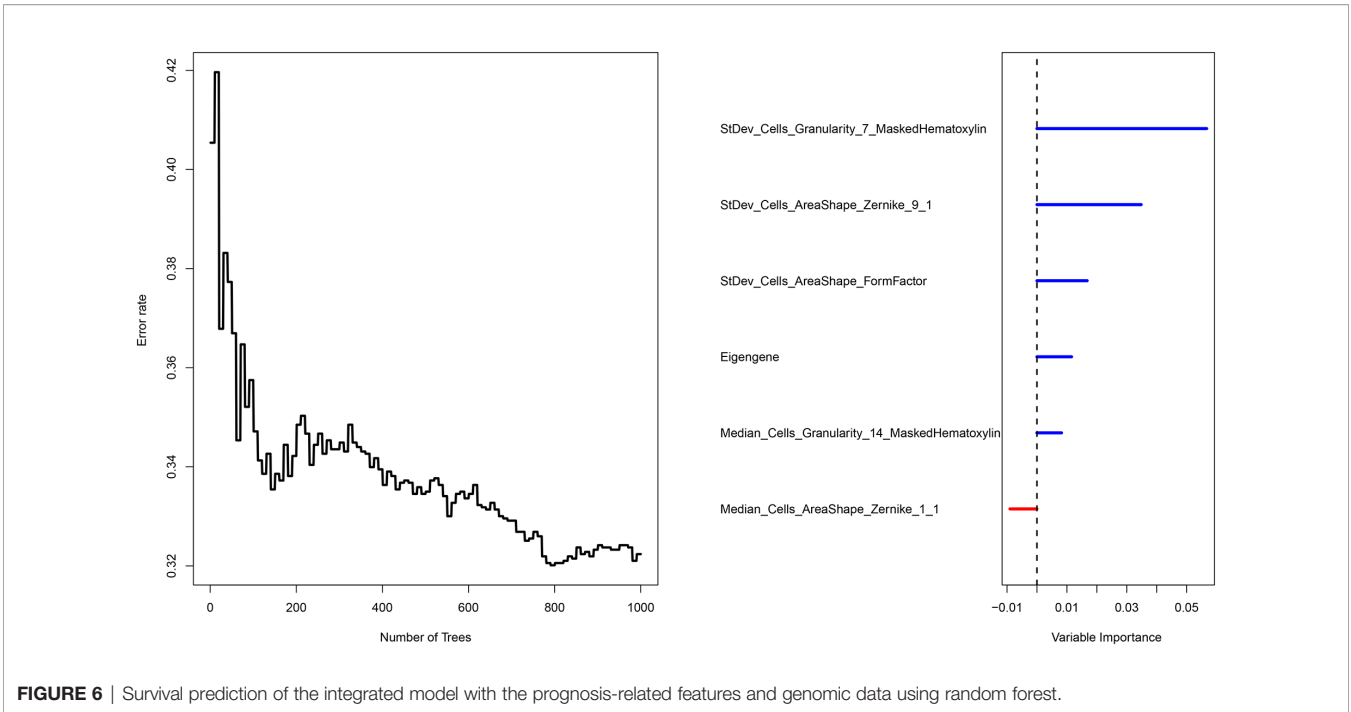


**FIGURE 6** | Survival prediction of the integrated model with the prognosis-related features and genomic data using random forest.

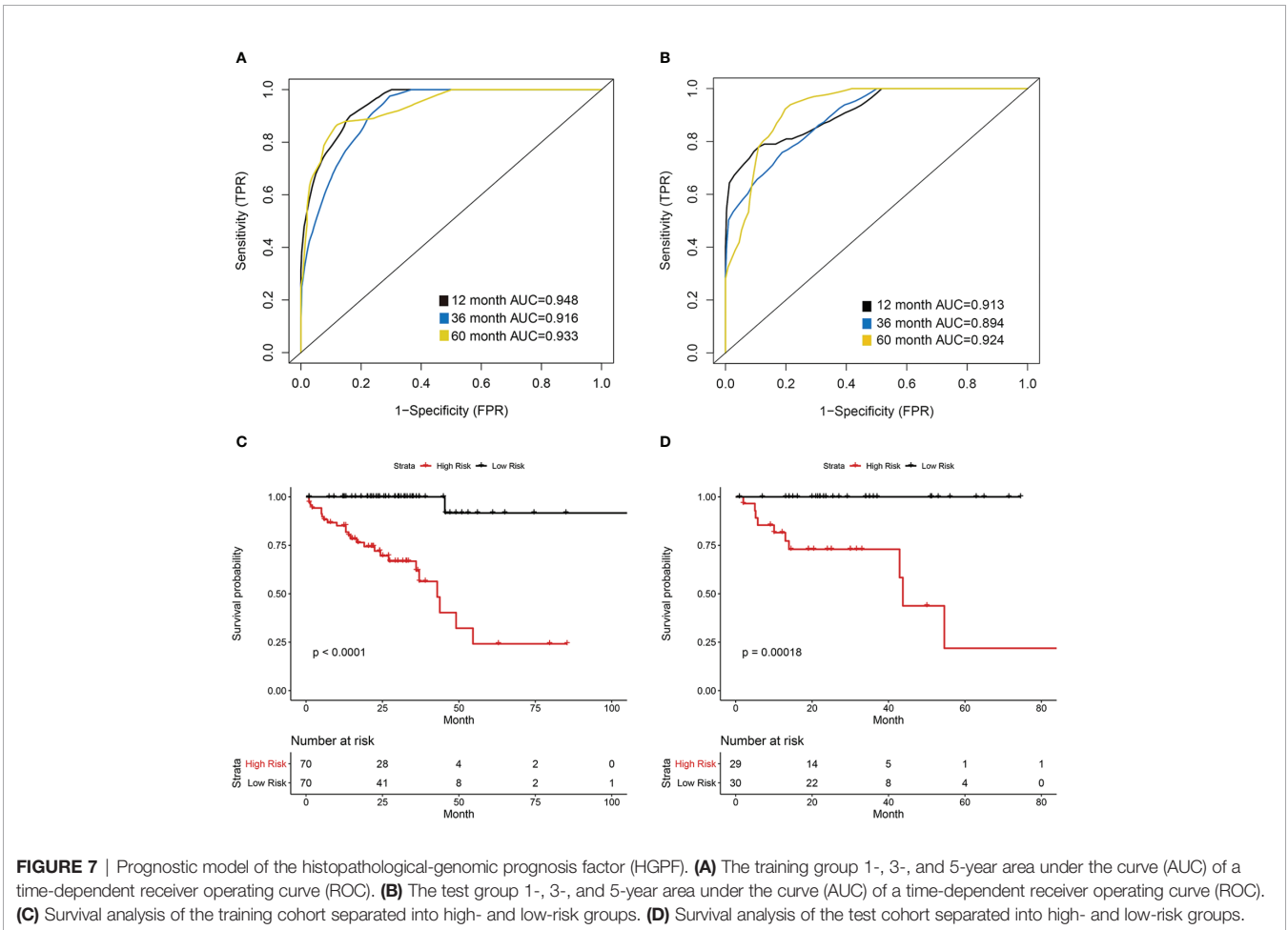
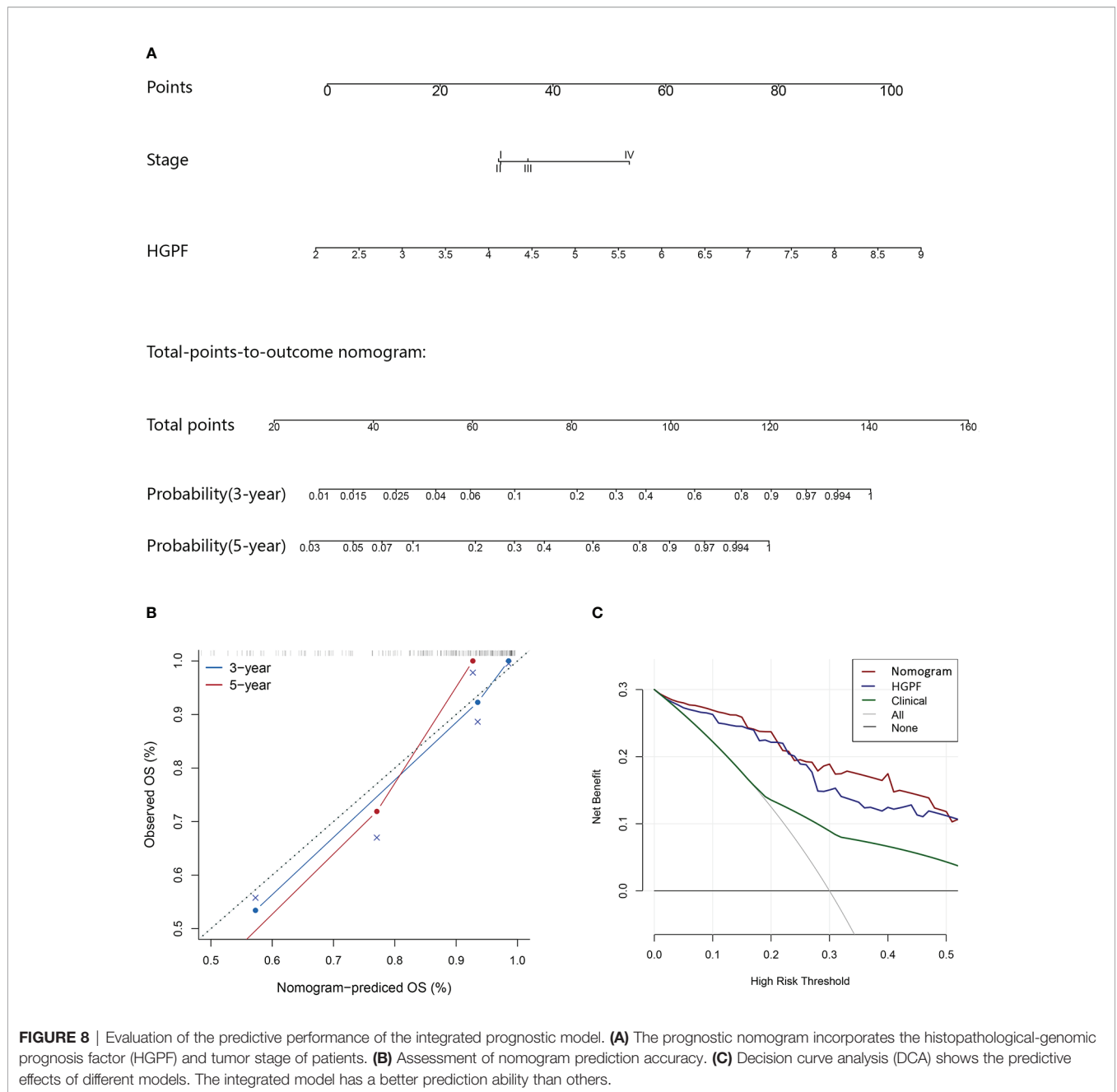


**FIGURE 7** | Prognostic model of the histopathological-genomic prognosis factor (HGPF). **(A)** The training group 1-, 3-, and 5-year area under the curve (AUC) of a time-dependent receiver operating curve (ROC). **(B)** The test group 1-, 3-, and 5-year area under the curve (AUC) of a time-dependent receiver operating curve (ROC). **(C)** Survival analysis of the training cohort separated into high- and low-risk groups. **(D)** Survival analysis of the test cohort separated into high- and low-risk groups.



prognosis-related module through enrichment analysis. Furthermore, the prognostic image features, co-expression gene module, and clinical information were integrated to construct a prognosis prediction model, which had a better prediction performance than other models. In summary, it is suggested that histopathological image features have a certain ability to predict patient survival, and multi-omics combination could further improve the prognosis prediction in COAD.

Our study identified five image features associated with the prognosis of COAD patients, including two Zernike shape features of the nuclei, two Granularity features, and a formfactor feature.

It can be inferred that the differences in the texture and morphology of the pathological images may influence the prognosis of COAD. In addition to prognosis prediction, the discrepancies in the cell structure revealed by these image features may lead to the differences in the invasion activity of tumor cells. In bladder cancer, a staging diagnostic model based on tumor invasiveness were developed with the histopathological image features (35). This approach can also be applied to the accurate grading of other cancers (36). It was difficult for pathologists to distinguish these image features by the naked eye. Therefore, the application of computer algorithms to identify the histopathological features

related to prognosis could reveal more underlying biological mechanisms of tumor development and progression in COAD.

After defining the prognostic image features, we constructed a gene co-expression network to identify the prognosis-related gene module and performed enrichment analysis to further explore the potential molecular pathways and mechanisms of genes in the brown module. Among the enriched signaling pathways, pathways associated with the tumor microenvironment were dominated such as ECM organization and blood vessel development. ECM is a key regulatory factor in the initiation of the TGF- $\beta$  signaling pathway, and can determine the outcomes of cytokine action, such as inducing the epithelial-mesenchymal transition (EMT) (37, 38). EMT was regarded as a pivotal step for cancer cells to acquire the ability of migration and invasion (39, 40). Moreover, the changes of ECM organization may play a crucial role in tumor recurrence and therapeutic resistance (41, 42). The rapid proliferation of cancer cells leads to the formation of hypoxic areas in the tumor center. The tumors facilitate angiogenesis for further growth, which, in return, increases the need for new blood vessels (43). Epithelial cells with EMT will lead to the reduction of cell junctions, recombination of the cytoskeleton structure, and changes in the cell polarity and cell shape, which may lead to characteristic changes in the histopathological images (44). Considering the correlation between the five prognosis-related features and co-expression gene module, these enriched signaling pathways may be potential biological mechanisms correlated with the prognosis-related histopathological image features.

Our research further established a robust prognostic model using prognostic image features, prognosis related co-expression gene module, and clinical characteristics of COAD patients. Many previous studies have conducted extensive investigation and modeling using single omics, such as genomic signatures of COAD (45–47). In this study, we integrated the pathological image features and genomics of COAD for the first time and improved the prediction performance of single-source prognostic models. This method of combining the pathological images with genomics to predict survival has been applied in other tumors (23, 48). Some studies also found that integrative models could improve the prediction performance of genomics and other images modalities, such as magnetic resonance imaging and computerized tomography (49–51). However, on account of the changes in tumor molecular mechanisms are often reflected in cell morphology, pathological images may have a better insight, interpretability, and sensitivity than radiomic images.

To our best knowledge, this was the first time that histopathological images and genomics were integrated to predict the prognosis of COAD patients. Our research exploited a new feasibility for establishing prognostic models of COAD with multi-

omics data, and conducted more utilization and excavation of histopathological image information. In addition, the analysis of signaling pathways may put forward a new direction for the potential biological mechanism of pathological morphological changes, which may provide a reference for the clinical prognosis and treatment strategies in COAD. However, this study still had some limitations and required further investigation. Although a significant prognostic value of the integrative model has been demonstrated in our validation, its accuracy and practicability still need to be verified by multi-center and large-scale studies. Secondly, the specific molecular mechanisms of the connection between the enriched signaling pathway and the prognostic model are still unclear and need further study.

## CONCLUSION

In conclusion, our study constructed a robust integrative model based on multi-omics features to predict the survival outcomes of patients with colon adenocarcinoma. This model deepened the cognition about the histopathological image information and may contribute to the clinical decision and treatment of colon adenocarcinoma. Moreover, the potential biological mechanisms of the histopathological image features affecting the survival outcomes need further exploration.

## DATA AVAILABILITY STATEMENT

The original contributions presented in the study are included in the article/**Supplementary Material**. Further inquiries can be directed to the corresponding author.

## AUTHOR CONTRIBUTIONS

HZ and HL are responsible for the conception and design of the research. LC is responsible for data downloading and sorting. HZ conducted the data processing. HL is responsible for editing the article and formatting. QL is in charge of the interpretation of data. JJ is in charge of submission and manuscript revision. All authors contributed to the article and approved the submitted version.

## SUPPLEMENTARY MATERIAL

The Supplementary Material for this article can be found online at: <https://www.frontiersin.org/articles/10.3389/fonc.2021.636451/full#supplementary-material>

## REFERENCES

1. Miller KD, Nogueira L, Mariotto AB, Rowland JH, Yabroff KR, Alfano CM, et al. Cancer Treatment and Survivorship Statistics, 2019. *CA Cancer J Clin* (2019) 69(5):363–85. doi: 10.3322/caac.21565
2. Labianca R, Beretta GD, Kildani B, Milesi L, Merlin F, Mosconi S, et al. Colon Cancer. *Crit Rev Oncol Hematol* (2010) 74(2):106–33. doi: 10.1016/j.critrevonc.2010.01.010
3. Dienstmann R, Salazar R, Tabernero J. Personalizing Colon Cancer Adjuvant Therapy: Selecting Optimal Treatments for Individual Patients. *J Clin Oncol* (2015) 33(16):1787–96. doi: 10.1200/JCO.2014.60.0213
4. Steinberg SM, Barkin JS, Kaplan RS, Stablein DM. Prognostic Indicators of Colon Tumors. The Gastrointestinal Tumor Study Group Experience. *Cancer* (1986) 57(9):1866–70. doi: 10.1002/1097-0142(19860501)57:9<1866::aid-cncr2820570928>3.0.co;2-t

5. Wilson ML, Fleming KA. Global Cancer Care: The Role of Pathology. *Am J Clin Pathol* (2016) 145(1):6–7. doi: 10.1093/ajcp/aqv030
6. Nelson AM, Milner DA, Rebbeck TR, Iliyasa Y. Oncologic Care and Pathology Resources in Africa: Survey and Recommendations. *J Clin Oncol* (2016) 34(1):20–6. doi: 10.1200/JCO.2015.61.9767
7. Hipp J, Flotte T, Monaco J, Cheng J, Madabhushi A, Yagi Y, et al. Computer Aided Diagnostic Tools Aim to Empower Rather Than Replace Pathologists: Lessons Learned From Computational Chess. *J Pathol Inform* (2011) 2:25. doi: 10.4103/2153-3539.82050
8. Beck AH, Sangoi AR, Leung S, Marinelli RJ, Nielsen TO, van de Vijver MJ, et al. Systematic Analysis of Breast Cancer Morphology Uncovers Stromal Features Associated With Survival. *Sci Transl Med* (2011) 3(108):108ra113. doi: 10.1126/scitranslmed.3002564
9. Yu KH, Zhang C, Berry GJ, Altman RB, Ré C, Rubin DL, et al. Predicting non-Small Cell Lung Cancer Prognosis by Fully Automated Microscopic Pathology Image Features. *Nat Commun* (2016) 7:12474. doi: 10.1038/ncomms12474
10. Luo X, Zang X, Yang L, Huang J, Liang F, Rodriguez-Canales J, et al. Comprehensive Computational Pathological Image Analysis Predicts Lung Cancer Prognosis. *J Thorac Oncol* (2017) 12(3):501–9. doi: 10.1016/j.jtho.2016.10.017
11. Zhao Y, Yang J, Luo M, Yang Y, Guo X, Zhang T, et al. Contrast-Enhanced CT-Based Textural Parameters as Potential Prognostic Factors of Survival for Colorectal Cancer Patients Receiving Targeted Therapy. *Mol Imaging Biol* (2021) 23(3):427–35. doi: 10.1007/s11307-020-01552-2
12. Wilkins A, Dearnaley D, Somaiah N. Genomic and Histopathological Tissue Biomarkers That Predict Radiotherapy Response in Localised Prostate Cancer. *BioMed Res Int* (2015) 2015:238757. doi: 10.1155/2015/238757
13. Taherian-Fard A, Srihari S, Ragan MA. Breast Cancer Classification: Linking Molecular Mechanisms to Disease Prognosis. *Brief Bioinform* (2015) 16(3):461–74. doi: 10.1093/bib/bbu020
14. Visser E, Franken IA, Broens LA, Ruurda JP, van Hillegersberg R. Prognostic Gene Expression Profiling in Esophageal Cancer: A Systematic Review. *Oncotarget* (2017) 8(3):5566–77. doi: 10.18632/oncotarget.13328
15. Xu Y, Zhong T, Wu M, Ma S. Histopathological Imaging-Environment Interactions in Cancer Modeling. *Cancers (Basel)* (2019) 11(4):579. doi: 10.3390/cancers11040579
16. Zhong T, Wu M, Ma S. Examination of Independent Prognostic Power of Gene Expressions and Histopathological Imaging Features in Cancer. *Cancers (Basel)* (2019) 11(3):361. doi: 10.3390/cancers11030361
17. Luo Y, Yang J, Yu J, Liu X, Yu C, Hu J, et al. Long Non-Coding RNAs: Emerging Roles in the Immunosuppressive Tumor Microenvironment. *Front Oncol* (2020) 10:48. doi: 10.3389/fonc.2020.00048
18. Yu KH, Berry GJ, Rubin DL, Ré C, Altman RB, Snyder M. Association of Omics Features With Histopathology Patterns in Lung Adenocarcinoma. *Cell Syst* (2017) 5(6):620–27.e3. doi: 10.1016/j.cels.2017.10.014
19. Cooper LA, Kong J, Gutman DA, Dunn WD, Nalisnik M, Brat DJ. Novel Genotype-Phenotype Associations in Human Cancers Enabled by Advanced Molecular Platforms and Computational Analysis of Whole Slide Images. *Lab Invest* (2015) 95(4):366–76. doi: 10.1038/labinvest.2014.153
20. Schiano C, Franzese M, Pane K, Garbino N, Soricelli A, Salvatore M, et al. Hybrid (18)F-FDG-PET/MRI Measurement of Standardized Uptake Value Coupled With Yin Yang 1 Signature in Metastatic Breast Cancer. A Preliminary Study. *Cancers (Basel)* (2019) 11(10):1444. doi: 10.3390/cancers11101444
21. Lin P, Wen DY, Chen L, Li X, Li SH, Yan HB, et al. A Radiogenomics Signature for Predicting the Clinical Outcome of Bladder Urothelial Carcinoma. *Eur Radiol* (2020) 30(1):547–57. doi: 10.1007/s00330-019-06371-w
22. Ma C, Yao Z, Zhang Q, Zou X. Quantitative Integration of Radiomic and Genomic Data Improves Survival Prediction of Low-Grade Glioma Patients. *Math Biosci Eng* (2020) 18(1):727–44. doi: 10.3934/mbe.2021039
23. Cheng J, Zhang J, Han Y, Wang X, Ye X, Meng Y, et al. Integrative Analysis of Histopathological Images and Genomic Data Predicts Clear Cell Renal Cell Carcinoma Prognosis. *Cancer Res* (2017) 77(21):e91–e100. doi: 10.1158/0008-5472.CCR-17-0313
24. Sun D, Li A, Tang B, Wang M. Integrating Genomic Data and Pathological Images to Effectively Predict Breast Cancer Clinical Outcome. *Comput Methods Programs BioMed* (2018) 161:45–53. doi: 10.1016/j.cmpb.2018.04.008
25. Shao W, Han Z, Cheng J, Cheng L, Wang T, Sun L, et al. Integrative Analysis of Pathological Images and Multi-Dimensional Genomic Data for Early-Stage Cancer Prognosis. *IEEE Trans Med Imaging* (2020) 39(1):99–110. doi: 10.1109/TMI.2019.2920608
26. Prior FW, Clark K, Commeyan P, Freymann J, Jaffe C, Kirby J, et al. TCIA: An Information Resource to Enable Open Science. *Annu Int Conf IEEE Eng Med Biol Soc* (2013) 2013:1282–5. doi: 10.1109/EMBC.2013.6609742
27. Clark K, Vendt B, Smith K, Freymann J, Kirby J, Koppel P, et al. The Cancer Imaging Archive (TCIA): Maintaining and Operating a Public Information Repository. *J Digit Imaging* (2013) 26(6):1045–57. doi: 10.1007/s10278-013-9622-7
28. Tomczak K, Czerwińska P, Wiznerowicz M. The Cancer Genome Atlas (TCGA): An Immeasurable Source of Knowledge. *Contemp Oncol (Pozn)* (2015) 19(1a):A68–77. doi: 10.5114/wo.2014.47136
29. Goode A, Gilbert B, Harkes J, Jukic D, Satyanarayanan M. OpenSlide: A Vendor-Neutral Software Foundation for Digital Pathology. *J Pathol Inform* (2013) 4:27. doi: 10.4103/2153-3539.119005
30. Soliman K. CellProfiler: Novel Automated Image Segmentation Procedure for Super-Resolution Microscopy. *Biol Proced Online* (2015) 17:11. doi: 10.1186/s12575-015-0023-9
31. Langfelder P, Horvath S. WGCNA: An R Package for Weighted Correlation Network Analysis. *BMC Bioinf* (2008) 9:559. doi: 10.1186/1471-2105-9-559
32. Zheng X, Huang R, Liu G, Jia Z, Chen K, He Y. Development and Verification of a Predictive Nomogram to Evaluate the Risk of Complicating Ventricular Tachyarrhythmia After Acute Myocardial Infarction During Hospitalization: A Retrospective Analysis. *Am J Emerg Med* (2021) 46:462–8. doi: 10.1016/j.ajem.2020.10.052
33. Li Q, Xiao Q, Li J, Duan S, Wang H, Gu Y. MRI-Based Radiomic Signature as a Prognostic Biomarker for HER2-Positive Invasive Breast Cancer Treated With NAC. *Cancer Manag Res* (2020) 12:10603–13. doi: 10.2147/CMAR.S271876
34. Wang P, Pei X, Yin XP, Ren JL, Wang Y, Ma LY, et al. Radiomics Models Based on Enhanced Computed Tomography to Distinguish Clear Cell From non-Clear Cell Renal Cell Carcinomas. *Sci Rep* (2021) 11(1):13729. doi: 10.1038/s41598-021-93069-z
35. Yin PN, Kc K, Wei S, Yu Q, Li R, Haake AR, et al. Histopathological Distinction of non-Invasive and Invasive Bladder Cancers Using Machine Learning Approaches. *BMC Med Inform Decis Mak* (2020) 20(1):162. doi: 10.1186/s12911-020-01185-z
36. Niazi MKK, Yao K, Zynger DL, Clinton SK, Chen J, Koyuturk M, et al. Visually Meaningful Histopathological Features for Automatic Grading of Prostate Cancer. *IEEE J BioMed Health Inform* (2017) 21(4):1027–38. doi: 10.1109/JBHI.2016.2565515
37. Cichon MA, Radisky DC. Extracellular Matrix as a Contextual Determinant of Transforming Growth Factor- $\beta$  Signaling in Epithelial-Mesenchymal Transition and in Cancer. *Cell Adh Migr* (2014) 8(6):588–94. doi: 10.4161/19336918.2014.972788
38. Stallings-Mann ML, Waldmann J, Zhang Y, Miller E, Gauthier ML, Visscher DW, et al. Matrix Metalloproteinase Induction of Rac1b, a Key Effector of Lung Cancer Progression. *Sci Transl Med* (2012) 4(142):142ra95. doi: 10.1126/scitranslmed.3004062
39. Yang J, Weinberg RA. Epithelial-Mesenchymal Transition: At the Crossroads of Development and Tumor Metastasis. *Dev Cell* (2008) 14(6):818–29. doi: 10.1016/j.devcel.2008.05.009
40. Strizzi L, Hardy KM, Seftor EA, Costa FF, Kirschmann DA, Seftor RE, et al. Development and Cancer: At the Crossroads of Nodal and Notch Signaling. *Cancer Res* (2009) 69(18):7131–4. doi: 10.1158/0008-5472.CAN-09-1199
41. Zhai X, Xue Q, Liu Q, Guo Y, Chen Z. Colon Cancer Recurrence-Associated Genes Revealed by WGCNA Co-Expression Network Analysis. *Mol Med Rep* (2017) 16(5):6499–505. doi: 10.3892/mmr.2017.7412
42. Ni Y, Zhou X, Yang J, Shi H, Li H, Zhao X, et al. The Role of Tumor-Stroma Interactions in Drug Resistance Within Tumor Microenvironment. *Front Cell Dev Biol* (2021) 9:637675. doi: 10.3389/fcell.2021.637675
43. Batlle R, Andrés E, Gonzalez L, Llonch E, Igea A, Gutierrez-Prat N, et al. Regulation of Tumor Angiogenesis and Mesenchymal-Endothelial Transition

- by P38 $\alpha$  Through TGF- $\beta$  and JNK Signaling. *Nat Commun* (2019) 10(1):3071. doi: 10.1038/s41467-019-10946-y
44. Lamouille S, Xu J, Derynck R. Molecular Mechanisms of Epithelial-Mesenchymal Transition. *Nat Rev Mol Cell Biol* (2014) 15(3):178–96. doi: 10.1038/nrm3758
45. Xu G, Zhang M, Zhu H, Xu J. A 15-Gene Signature for Prediction of Colon Cancer Recurrence and Prognosis Based on SVM. *Gene* (2017) 604:33–40. doi: 10.1016/j.gene.2016.12.016
46. Yang H, Liu H, Lin HC, Gan D, Jin W, Cui C, et al. Association of a Novel Seven-Gene Expression Signature With the Disease Prognosis in Colon Cancer Patients. *Aging (Albany NY)* (2019) 11(19):8710–27. doi: 10.18632/aging.102365
47. Gao P, He M, Zhang C, Geng C. Integrated Analysis of Gene Expression Signatures Associated With Colon Cancer From Three Datasets. *Gene* (2018) 654:95–102. doi: 10.1016/j.gene.2018.02.007
48. Hao J, Kosaraju SC, Tsaku NZ, Song DH, Kang M. PAGE-Net: Interpretable and Integrative Deep Learning for Survival Analysis Using Histopathological Images and Genomic Data. *Pac Symp Biocomput* (2020) 25:355–66. doi: 10.1142/9789811215636\_0032
49. Lee J, Li B, Cui Y, Sun X, Wu J, Zhu H, et al. A Quantitative CT Imaging Signature Predicts Survival and Complements Established Prognosticators in Stage I Non-Small Cell Lung Cancer. *Int J Radiat Oncol Biol Phys* (2018) 102(4):1098–106. doi: 10.1016/j.ijrobp.2018.01.006
50. Toledano MN, Desbordes P, Banjar A, Gardin I, Vera P, Ruminy P, et al. Combination of Baseline FDG PET/CT Total Metabolic Tumour Volume and Gene Expression Profile Have a Robust Predictive Value in Patients With Diffuse Large B-Cell Lymphoma. *Eur J Nucl Med Mol Imaging* (2018) 45(5):680–8. doi: 10.1007/s00259-017-3907-x
51. Shu C, Wang Q, Yan X, Wang J. The TERT Promoter Mutation Status and MGMT Promoter Methylation Status, Combined With Dichotomized MRI-Derived and Clinical Features, Predict Adult Primary Glioblastoma Survival. *Cancer Med* (2018) 7(8):3704–12. doi: 10.1002/cam4.1666

**Conflict of Interest:** The authors declare that the research was conducted in the absence of any commercial or financial relationships that could be construed as a potential conflict of interest.

**Publisher's Note:** All claims expressed in this article are solely those of the authors and do not necessarily represent those of their affiliated organizations, or those of the publisher, the editors and the reviewers. Any product that may be evaluated in this article, or claim that may be made by its manufacturer, is not guaranteed or endorsed by the publisher.

Copyright © 2021 Li, Chen, Zeng, Liao, Ji and Ma. This is an open-access article distributed under the terms of the Creative Commons Attribution License (CC BY). The use, distribution or reproduction in other forums is permitted, provided the original author(s) and the copyright owner(s) are credited and that the original publication in this journal is cited, in accordance with accepted academic practice. No use, distribution or reproduction is permitted which does not comply with these terms.